Friction Reduction by Superhydrophobic Surface

by **H. Isshiki and B. S. Yoon**
Univ. of Ulsan

Syra at Ofuna Campus of Kamakura Women's University
Dec. 5, 2009

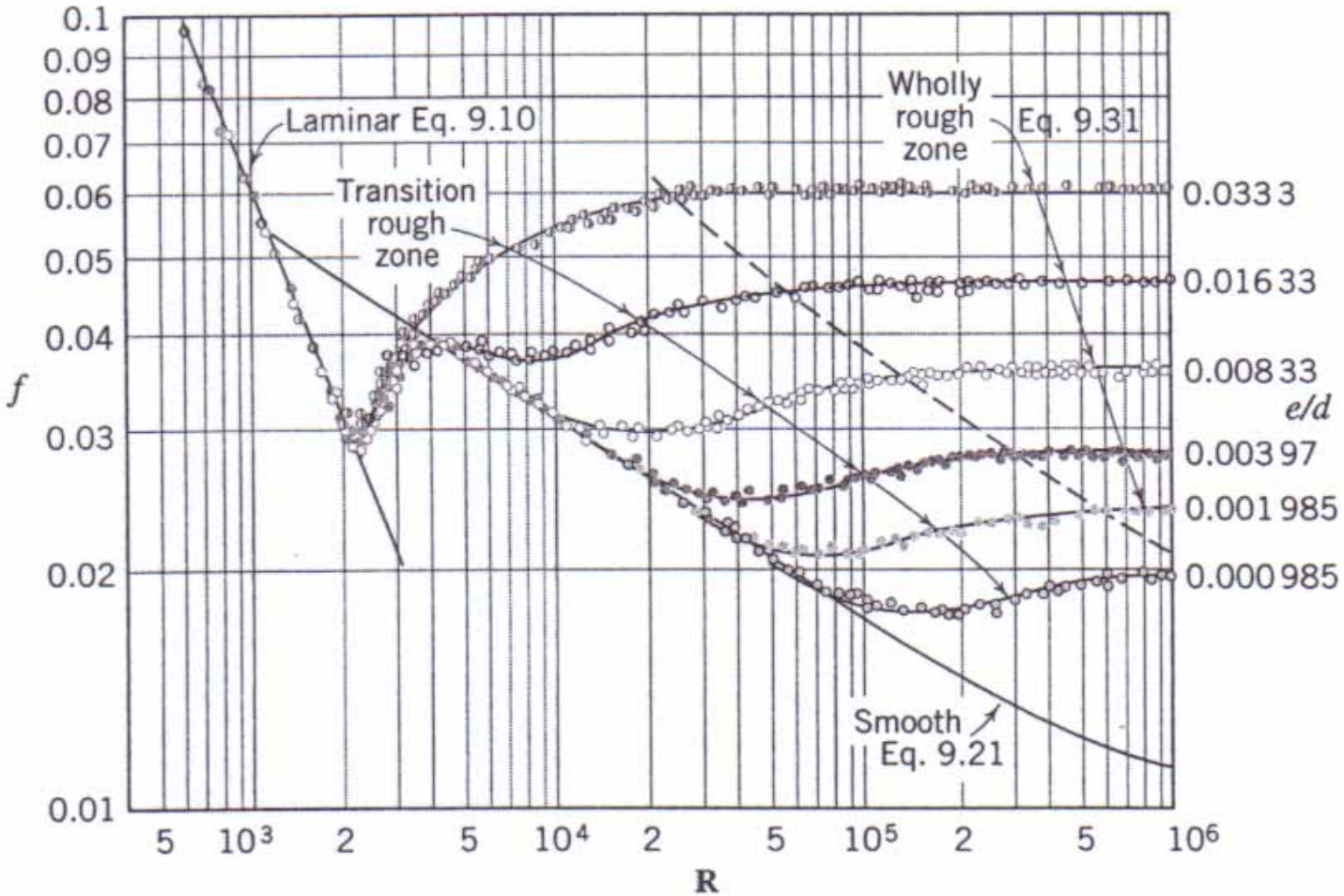

Nikuradse's experimental data (R. L. Street, et al., Elementary Fluid Mechanics, John Willey & Sonsp.345)

As the roughness increases, the friction increases.

Superhydrophobic surfaces shows smaller friction.

1. Property of Surface [1]

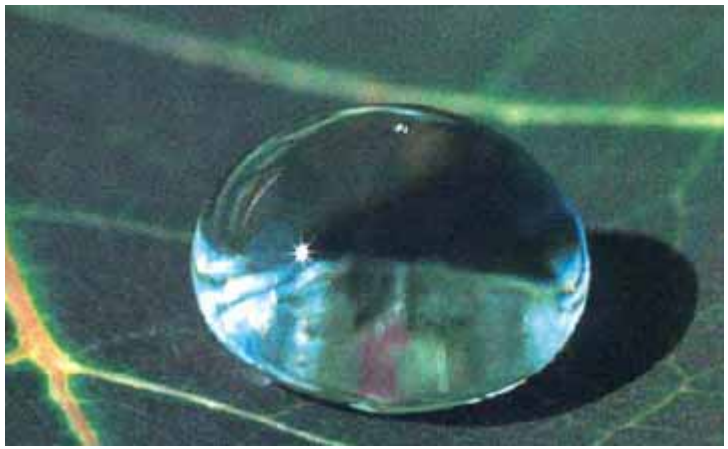

Self cleaning of
lotus leaf

Image of friction reduction

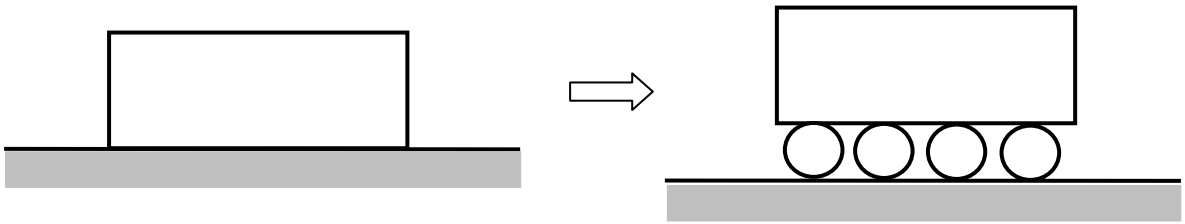

Friction between solids

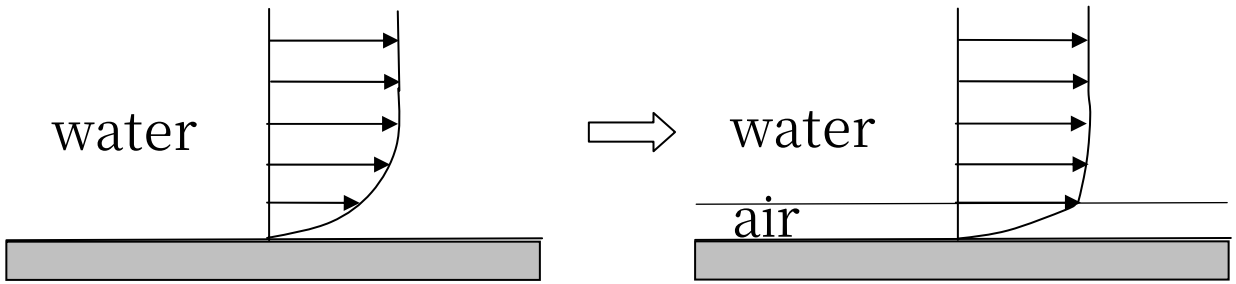

Friction between solid and water

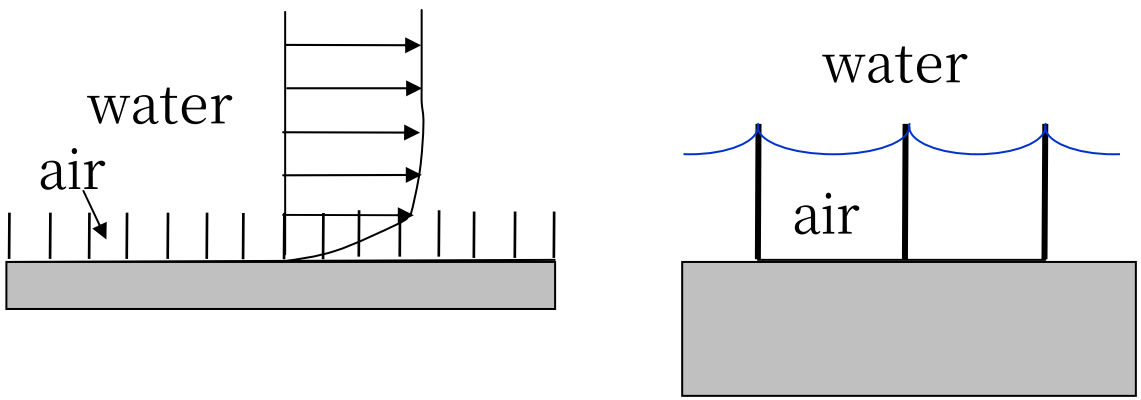

Air trapped on surface

Surface energy

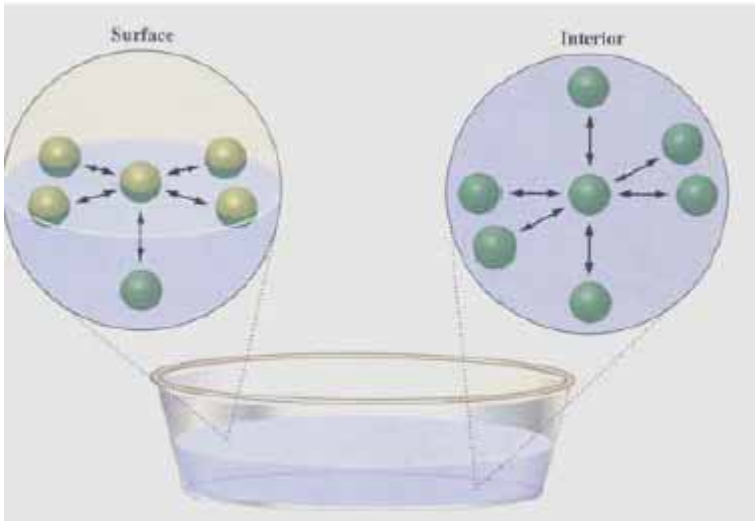

Energy of molecules at the interface > that in the liquid

Surface energy = Excess free energy per unit area of the interface

Surface tension (N/m) = Surface energy (J/m^2)

Hydrophilicity: Wettable property

Cleaning of surface

High thermal conductivity → Heat exchanger

Hydrophobicity: Water repulsive property

Self cleaning

Low frictional resistance

Anti-biofouling

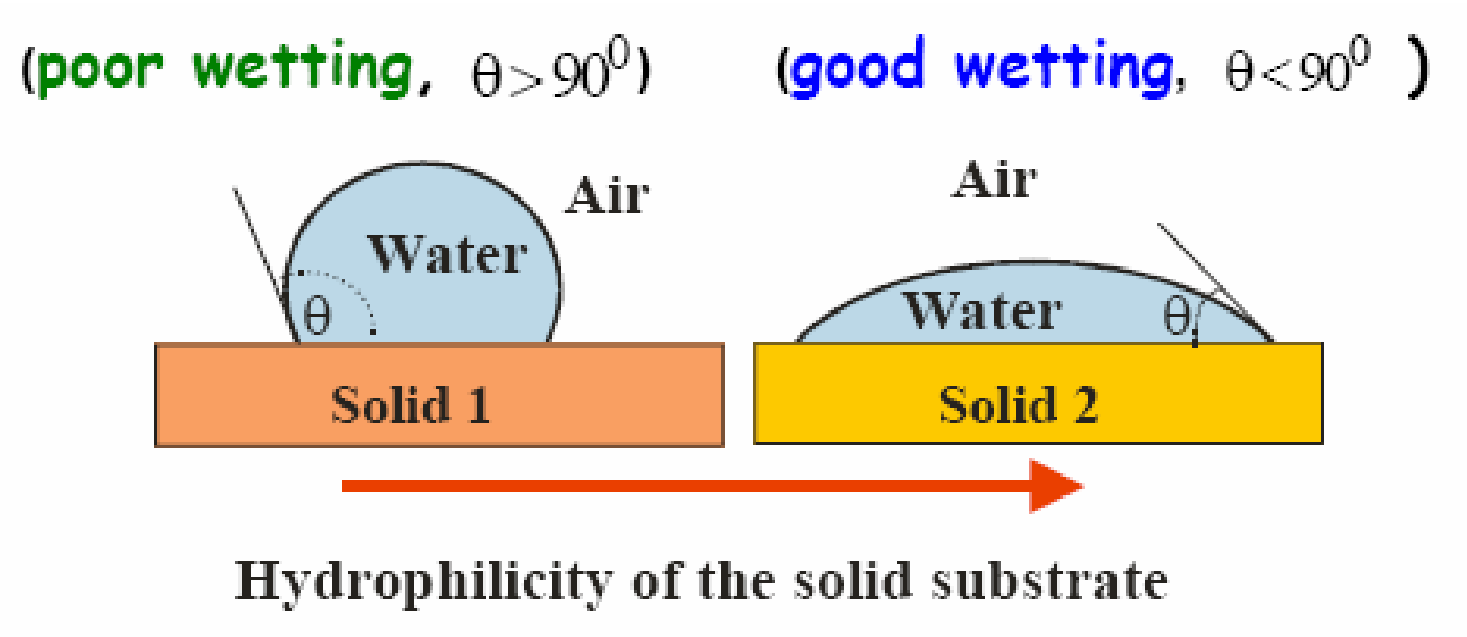

Young's equation (1807)

Three-phase contact angle

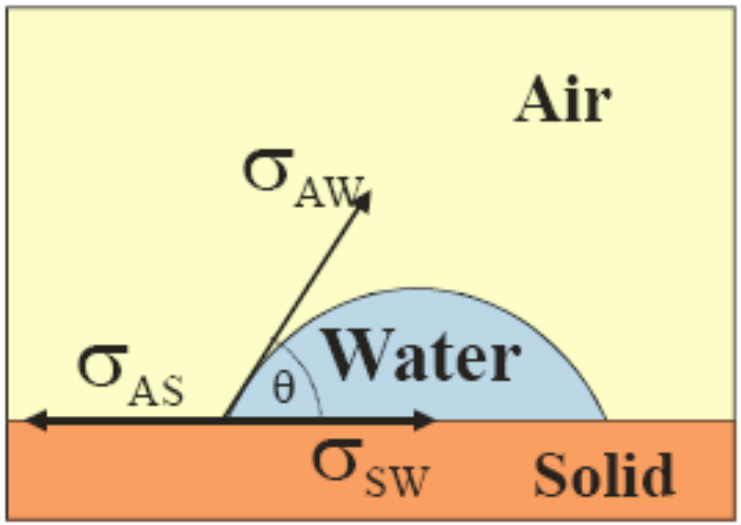

$$\sigma_{AS} = \sigma_{SW} + \sigma_{AW} \cos\theta$$

This equation can be derived strictly by a variational principle.

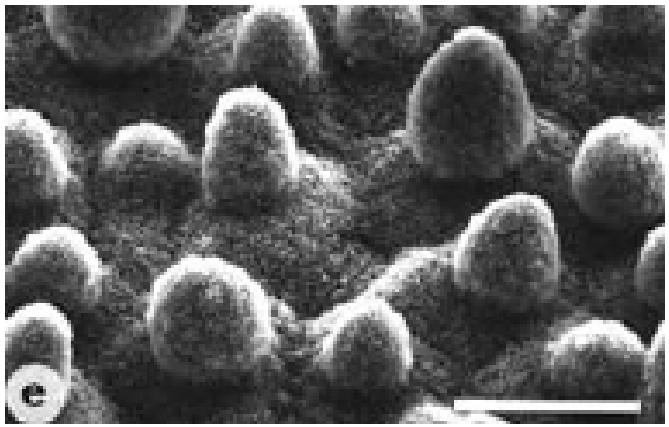

Lotus effect
Barthlott & Neinhuis
(Planta, 1997)

Super or Ultra hydrophobicity:
Contact angle ~180deg

Superhydrophobicity:
Hydrophobicity + Special structure

If the surface has a low interfacial free energy, liquid will accumulate within the corrugation and roughness promotes wetting.

For high energy surface, it becomes energetically expensive for the liquid to follow the surface corrugations and roughness promotes drying.

Cassie-Baxter-Good equation (1944)

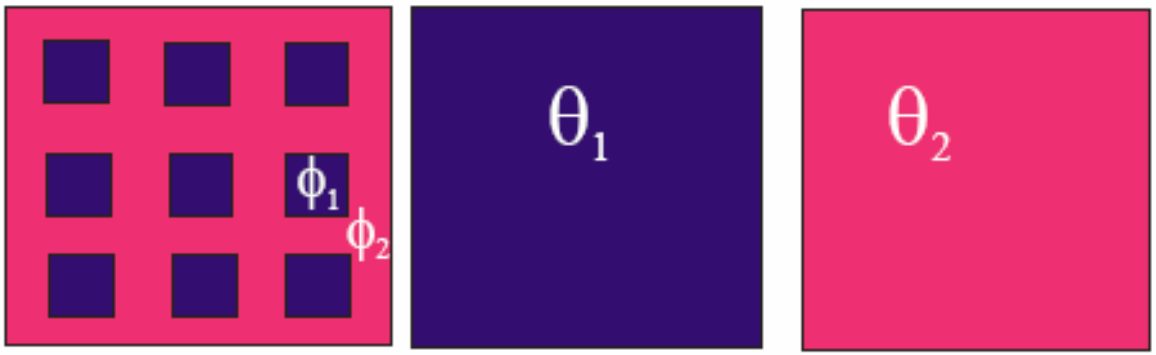

$$\cos\theta^* = \phi_1 \cos\theta_1 + \phi_2 \cos\theta_2$$

Obtained from Young's eq.

ϕ_1 and ϕ_2 : surface fractions of domain 1 and 2

θ_1 and θ_2 : contact angles of the surfaces

θ^* : apparent contact angle of the surface

When $\theta_2 = 180°$, $\cos\theta^* = -\phi_2 + \phi_1 \cos\theta_1$

If $\phi_1 << 1$ and $\phi_2 \approx 1$, then $\theta^* \approx 180°$

2. Friction Reduction by SHP

Present status:

(1) Superhydrophobicity brings in Friction reduction.

(2) Air layer is formed on the surface.

(3) Slip on water-air interface reduces friction.

(3) Even for turbulent flow, more effective.

(4) As Reynolds number higher, more effective.

(5) DNS calculations give some useful results.

(6) Relationship between slip length and details of surface structure is not well known.

(7) Robust structure seems possible.

2. Friction Reduction of Turbulent Pipe Flow by UOU [4,5]

2.1. Basic equations for turbulent flow in a pipe

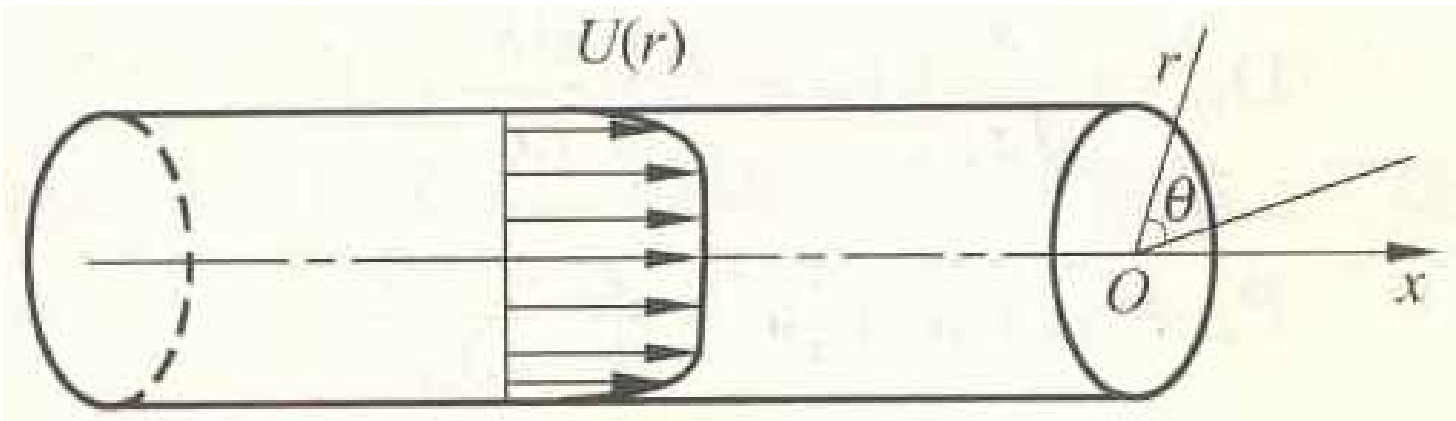

Figure 3.8. Turbulent flow in a pipe.

(1) The mean velocity field is a stationary and parallel flow.
(2) Except the pressure, the mean quantities are functions of the radial coordinates alone.

The mean flow in the pipe has the following properties:

$$\left(\langle U_r \rangle, \langle U_\theta \rangle, \langle U_x \rangle\right) = \left(0, 0, U(r)\right) \tag{1a}$$

$$\frac{\partial R_{ij}}{\partial x} = \frac{\partial R_{ij}}{\partial \theta} = 0 \tag{1b}$$

$$\langle p \rangle = p(r, x) \tag{1c}$$

Reynolds averaged equation:

$$\frac{1}{\rho}\frac{\partial p}{\partial x} = -\frac{1}{r}\frac{d}{dr}\left(r\langle u_r' u_x' \rangle\right) + \nu\left(\frac{d^2 U}{dr^2} + \frac{1}{r}\frac{dU}{dr}\right) \tag{2a}$$

$$\frac{1}{\rho}\frac{\partial p}{\partial r} = -\frac{1}{r}\frac{d}{dr}\left(r\langle u_r'^2 \rangle\right) + \frac{\langle u_\theta'^2 \rangle}{r} \tag{2b}$$

The boundary conditions:

In case of stream-wise slip l_x

$$\left\langle u'^2_r \right\rangle = \left\langle u'_r u'_x \right\rangle = 0 \qquad (3a)$$

$$U = -l_x \frac{dU}{dr} \qquad (3b)$$

Integrating eq. (2b)

$$p(x,r) + \rho\left\langle u'^2_r \right\rangle + \rho\int_R^r \left(\frac{\left\langle u'^2_r \right\rangle - \left\langle u'^2_\theta \right\rangle}{r} \right) dr = p_w(x) \qquad (4)$$

Differentiating eq. (4)

$$\frac{\partial p}{\partial x} = \frac{d\, p_w}{d\, x} \qquad (5)$$

Substitting this eq. into eq. (2a)

$$\frac{1}{\rho}\frac{d\,p_w}{d\,x} = -\frac{1}{r}\frac{d}{d\,r}\left(r\left\langle u_r' u_x' \right\rangle\right) + \nu\left(\frac{d^2 U}{d\,r^2} + \frac{1}{r}\frac{dU}{d\,r}\right) \tag{6}$$

Now, we integrate with respect to r , we derive

$$\frac{r}{2}\frac{d\,p_w}{d\,x} = -\rho\left\langle u_r' u_x' \right\rangle + \mu\frac{dU}{d\,r} \tag{7}$$

Since $\mu\, dU/dr = \tau_w$

$$\frac{d\,p_w}{d\,x} = \frac{4\tau_w}{D} \tag{8}$$

Hence

$$\frac{2r\tau_w}{D} = -\rho\left\langle u_r' u_x' \right\rangle + \mu\frac{dU}{d\,r} \tag{9}$$

Coordinates from the wall:

$$y = R - r \tag{10}$$

Friction velocity u_τ :

$$u_\tau^2 = \frac{|\tau_w|}{\rho} \quad \text{or} \quad u_\tau^2 = \frac{-\tau_w}{\rho} \tag{11}$$

Eq. (9) becomes

$$\left\langle u_y' u_x' \right\rangle - \nu \frac{dU}{dy} = +\frac{1}{\rho}\left(1 - \frac{y}{R}\right)\tau_w = -\left(1 - \frac{y}{R}\right)u_\tau^2 \tag{12}$$

The total shear stress decreases linearly to zero at the axis.

Making the above equation non-dimensional

$$\frac{\left\langle u_y' u_x' \right\rangle}{u_\tau^2} - \frac{dU^+}{d\,y^+} = \bar{y} - 1 \qquad (13)$$

where $U^+ = \frac{U}{u_\tau}$, $y^+ = \frac{y u_\tau}{\nu}$, $\bar{y} = \frac{y}{R}$ (14)

Relation between y^+ and $\bar{y}$

$$\frac{y^+}{\bar{y}} = \frac{u_\tau R}{\nu} >> 1 \qquad (15)$$

2.2. Sub-layer model close to pipe wall

At the thin layer close to the wall

$$\bar{y} = y/R << 1 \quad \text{and} \quad 1 - y/R \approx 1\,, \tag{16}$$

the total shear stress is equal to the wall shear stress approximately (→ eq. (12)).

$$-\mu \frac{dU}{dy} + \rho \left\langle u_y' u_x' \right\rangle = \tau_w, \ \text{when} \quad \bar{y} = y/R << 1 \tag{17}$$

Usually, the approximation of the equal shear stress layer may reach $\bar{y} \approx 0.2 \sim 0.3$.

(1) Linear sub-layer

In a region very close to the wall, the pulsating component of the turbulent flow is very small, and $\left\langle u_x' u_y' \right\rangle \approx 0$.

$$\frac{dU^+}{dy^+} = 1 \tag{18}$$

Because of the boundary condition:

$$U = l_x \frac{dU}{dy} \quad \text{or} \quad U^+ = \frac{u_\tau l_x}{\nu} \frac{dU^+}{dy^+} = \frac{u_\tau l_x}{\nu} = l_x^+ \tag{19}$$

Hence

$$U^+ = y^+ + \frac{u_\tau l_x}{\nu} = y^+ + l_x^+ \tag{20}$$

The vast amount of the experimental data tell us that the linear distribution is a very good approximation when $y^+ < 5$.

(2) Logarithmic layer

In the region with $\bar{y} << 1$ and $y^+ >> 1$ outside the sub-layer, the molecular viscosity may be neglected.

This layer is called Reynolds stress layer.

After neglecting, dU^+/dy^+, equation (17) is simplified as

$$\left\langle u_r' u_x' \right\rangle = -u_\tau^2 \tag{21}$$

Substituting the mixed length model:

$$\left\langle u_y' u_x' \right\rangle = -\nu_T \frac{dU}{dy}, \quad \nu_T = k^2 y^2 \left| \frac{dU}{dy} \right| \tag{22}$$

We have

$$k^2 y^2 \left(\frac{dU}{dy} \right)^2 = u_\tau^2 \tag{23}$$

or

$$\frac{dU^+}{dy^+} = \frac{1}{k y^+} \tag{24}$$

Eq. (24) gives logarithmic velocity distribution. The integral constant must reflect the slip.

$$U^+ = \frac{1}{k}\ln y^+ + B + F \tag{25}$$

$$k = 0.4, \quad B = 5.5 \tag{26}$$

The DNS results by Choi & Kim and Fulagata, Kasagi et al. give very important information on this problem.

F is a function of stream-wise slip l_x^+ and span-wise slip l_θ^+.

DNS result by Choi and Kim on vel. dist. $U^+ - U_s^+$

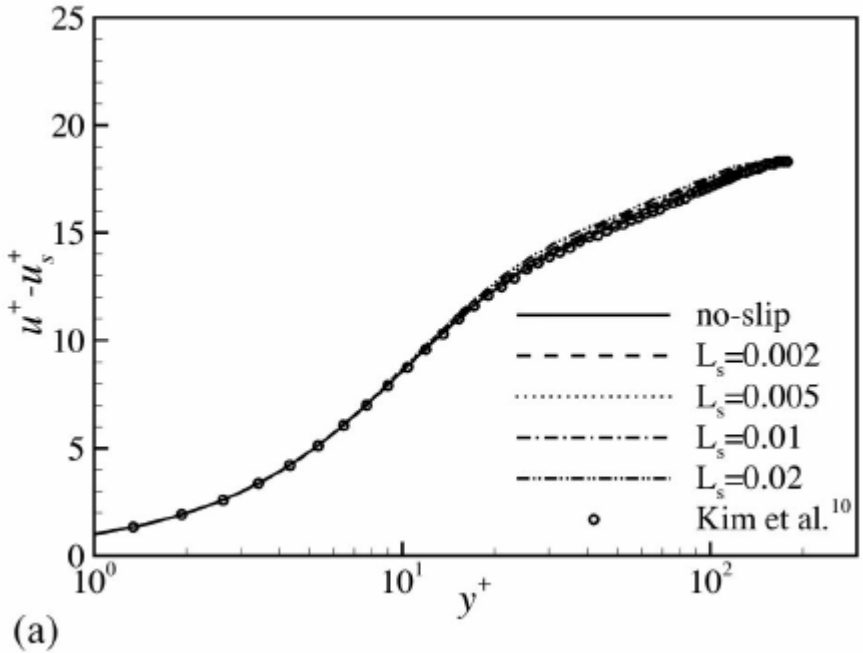

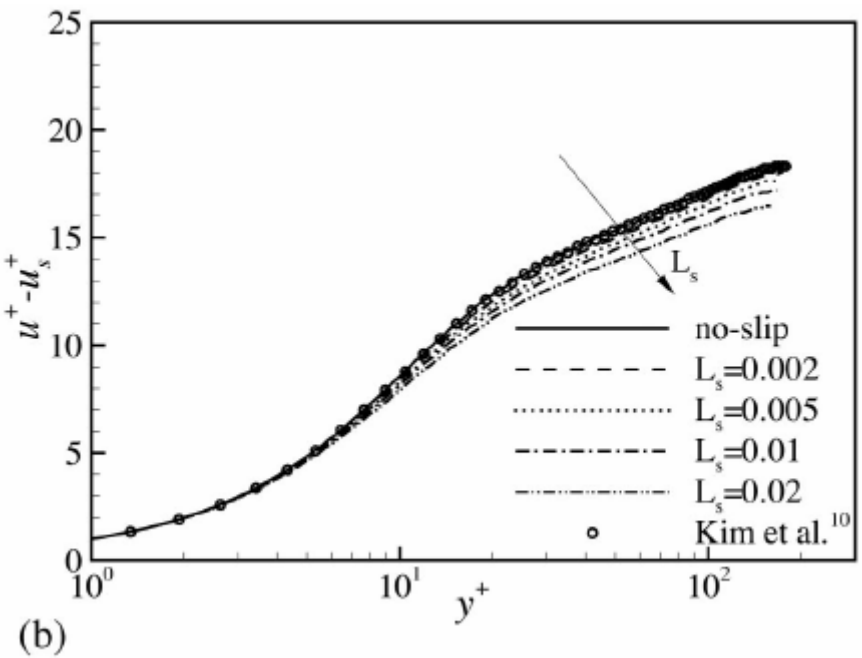

Fig. Mean velocity profiles $U^+ - U_s^+$:
(a) Case 1, stream-wise slip;
(b) Case 2, span-wise slip.

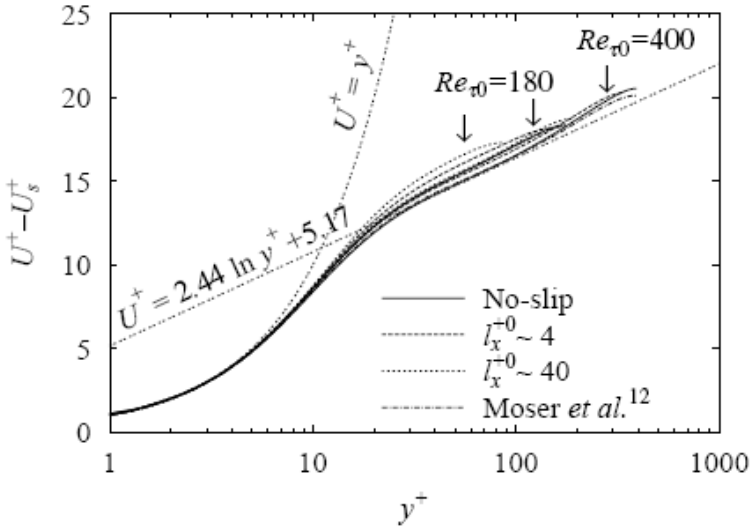

DNS result by Fukagata and Kasagi et al. on vel. dist.

$U^+ - U_s^+$

FIG. 1: Streamwise slip case: (a) mean velocity profile (keys of $l_x^{+0} \sim 4$ and 40 represent, respectively, $l_x^{+0} \simeq 3.6$ and 36 at $Re_{\tau 0} \simeq 180$, $l_x^{+0} \simeq 4.0$ and 40 at $Re_{\tau 0} \simeq 400$); (b) schematics of the drag decrease mechanism[8] and the effective bulk mean velocity, U_{be}.

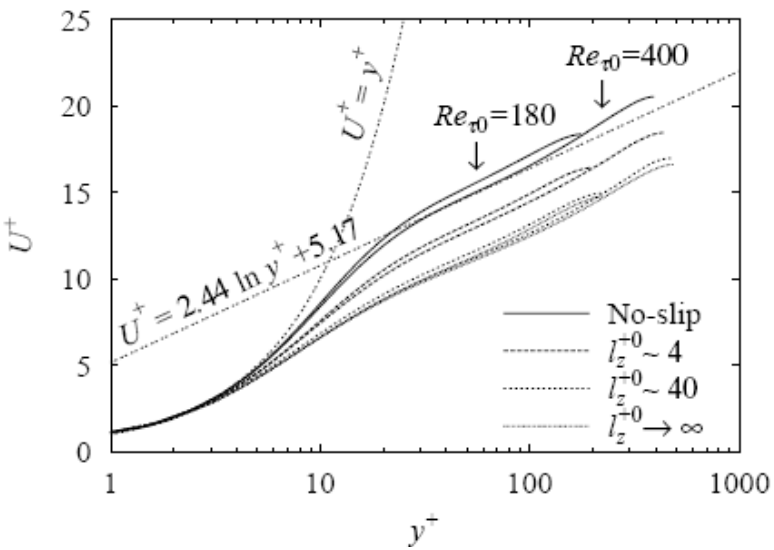

FIG. 2: Spanwise slip case: (a) mean velocity profile; (b) drag increase mechanism.[8]

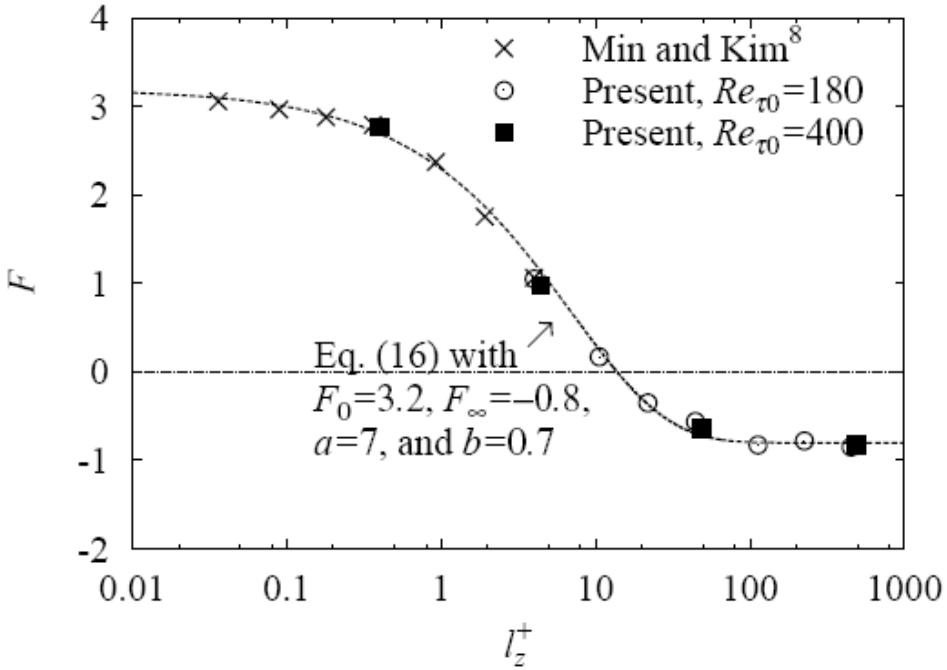

Estimation of F by Fukagata and Kasagi et al.

FIG. 3: Curve fit of $F(l_z^+)$.

When $l_z^+ = 0$, $F = l_x^+$.
This corresponds to the boundary condition (19): $U^+ = l_x^+$.
So, this may be correct for the pipe flow too.

From the above figure

$$F(l_x^+, l_z^+) = F_\infty + \left(l_x^+ - F_\infty\right)\exp\left[-\left(\frac{l_z^+}{a}\right)^b\right] \quad (27)$$

$$F_\infty = 0.8, \quad a = b = 0.7 \quad (28)$$

F_∞, a and b are obtained by DNS at $\mathrm{Re}_{\tau 0} = 180$ and 400 for a rectangular channel.

(3) Buffering zone

The region $5 < y_+ < 30$ is called the buffering zone.

An approximate expression may be given by

$$U^+ = 5\ln y^+ - 3.05 + F \tag{29}$$

(4) Center zone

The region $\bar{y} > (0.3 \sim 0.4)$ is called the center zone.

An approximate expression may be given by

$$\frac{U_{\max} - U(\bar{y})}{u_\tau} = -2.44\ln \bar{y} + 0.8 \tag{30}$$

2.3. Average velocity of the cross section

By integrating the velocity distributions of each layer, we can obtain the average U_m over the cross section of the mean velocity.

Practically, we integrate the velocity distribution in the logarithmic layer, since the singularity at zero is integrable, the volume flow below the buffering region is very small and the velocity calculated by the logarithmic distribution is close to the velocity in the central region.

So, the average velocity is obtained by integrating the logarithmic distribution.

From eq. (25), the velocity distribution is given by

$$\frac{U}{u_\tau} = \frac{1}{k}\ln y + \frac{1}{k}\ln\frac{u_\tau}{\nu} + B + F \qquad (31)$$

Integrating this eq.

$$\frac{U_m}{u_\tau} = \frac{1}{u_\tau}\frac{1}{\pi R^2}\int_0^R U\, 2\pi r dr$$

$$= \frac{1}{k}\frac{1}{\pi R^2}\int_0^R \ln(R-r)\, 2\pi r dr + \frac{1}{k}\ln\frac{u_\tau}{\nu} + B + F$$

$$= \frac{1}{k}\ln\frac{u_\tau R}{\nu} - \frac{3}{2}\frac{1}{k} + B + F \qquad (32)$$

Substituting (26), we have

$$\boxed{\frac{U_m}{u_\tau} = 2.5\ln\frac{u_\tau R}{\nu} + 1.75 + F} \qquad (33)$$

2.4. Drag coefficient for turbulent flow in a pipe

We define two kinds of non-dimensional drag coefficients.

The non-dimensional mean shear stress coefficient C_f :

$$C_f = \frac{-\tau_w}{\rho U_m^2 / 2} \tag{34}$$

The non-dimensional mean pressure gradient coefficient λ :

$$\lambda = -\frac{D}{\rho U_m^2 / 2}\frac{dp_w}{dx} \tag{35}$$

The relationship between the mean pressure drop and the mean shear stress:

$$\frac{dp_w}{dx} = \frac{4\tau_w}{D} \tag{8}$$

So $\lambda = 4 C_f$ (36)

From equations (8) and (11), we obtain an formula for the drag coefficient:

$$\lambda = -\frac{D}{\rho U_m^2/2}\frac{d p_w}{d x} = \frac{8u_\tau^2}{U_m^2} \tag{37}$$

Or $$\frac{u_\tau}{U_m} = \frac{\sqrt{\lambda}}{2\sqrt{2}} \tag{38}$$

If the mean velocity formula (32) is substituted into eq. (37), the drag coefficient can be written as

$$\lambda = \frac{8u_\tau^2}{U_m^2} = 8\Big/\left(\frac{1}{k}\ln\frac{u_\tau R}{\nu} - \frac{3}{2}\frac{1}{k} + B + F\right)^2 \tag{39}$$

where $$\frac{u_\tau R}{\nu} = \frac{u_\tau}{U_m}\frac{U_m R}{\nu} = \frac{u_\tau}{2U_m} Re = Re\frac{\sqrt{\lambda}}{4\sqrt{2}} \tag{40}$$

So, if Re is given, we can obtain λ by solving an implicit algebraic equation (39) for λ by iteration method.

Solution by iteration

From eqs. (39) and (27)

$$\lambda = \frac{8u_\tau^2}{U_m^2} = 8 \Bigg/ \left[\frac{1}{k} \ln\left(Re \frac{\sqrt{\lambda}}{4\sqrt{2}} \right) - \frac{3}{2}\frac{1}{k} + B + F \right]^2 \qquad (41)$$

where $F = F_\infty + \left(\mathrm{Re} \frac{\sqrt{\lambda}}{4\sqrt{2}} \frac{l_x}{R} - F_\infty \right) \exp\left[-\left(\frac{1}{a} \mathrm{Re} \frac{\sqrt{\lambda}}{4\sqrt{2}} \frac{l_z}{R} \right)^b \right]$ (42)

If we define $X = Re \frac{\sqrt{\lambda}}{4\sqrt{2}} \left(= \frac{u_\tau R}{\nu} \right)$ (43)

$$X = \frac{Re}{2\left(\frac{1}{k} \ln X - \frac{3}{2}\frac{1}{k} + B + F \right)}, \quad F = F_\infty + \left(X \frac{l_x}{R} - F_\infty \right) \exp\left[-\left(\frac{1}{a} X \frac{l_z}{R} \right)^b \right] \qquad (44)$$

2.5. Numerical calculations

$(a)\ \ l_x = 10\mu m; l_z = 0$

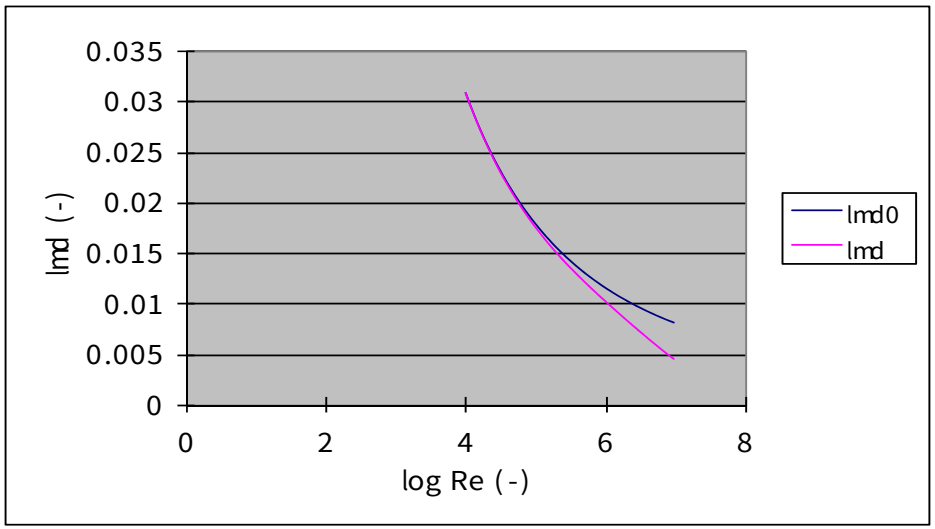

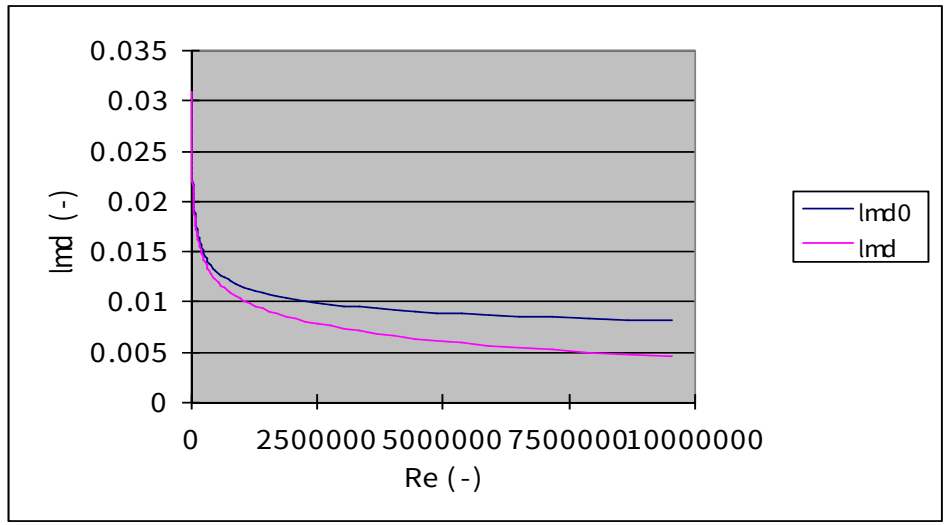

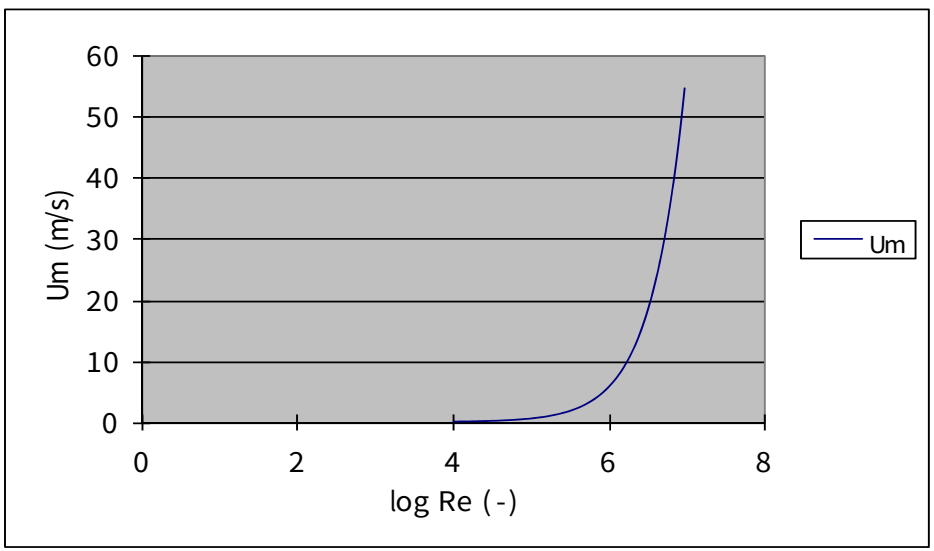

Drag reduction by slip

$(R = 10cm; \nu = 1.14 \times 10^{-6}\ m^2/s;$
$l_x = 10\mu m; l_z = 0)$

$(b)\ \ l_x = 10\mu m;\ l_z = 0$

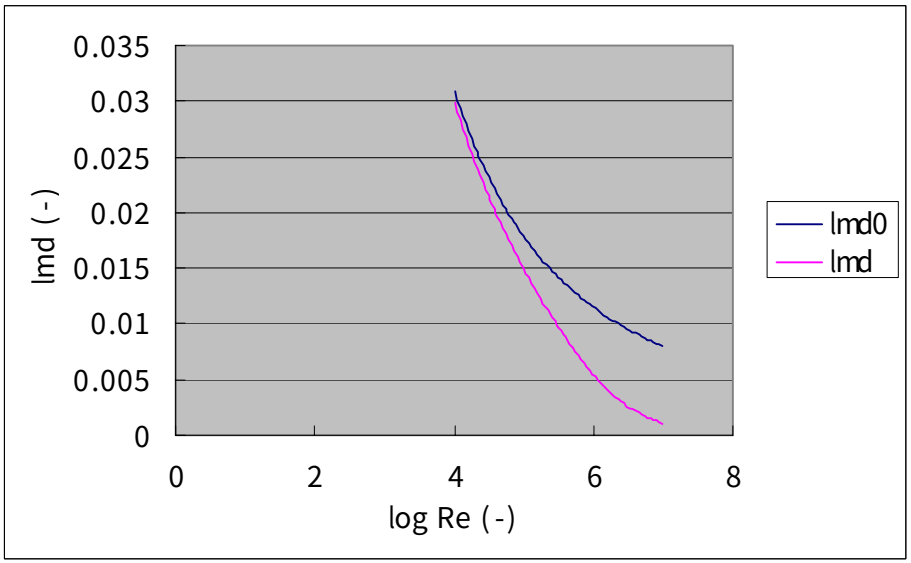

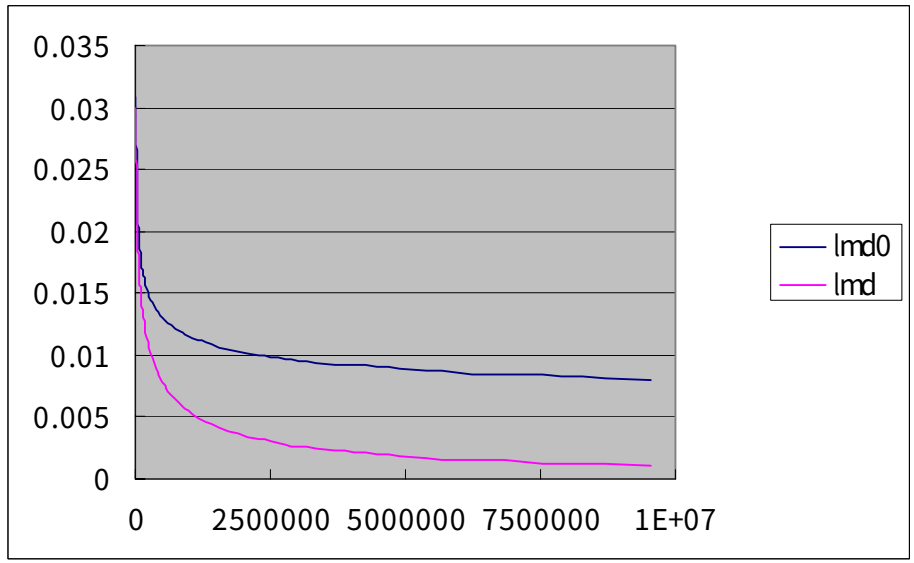

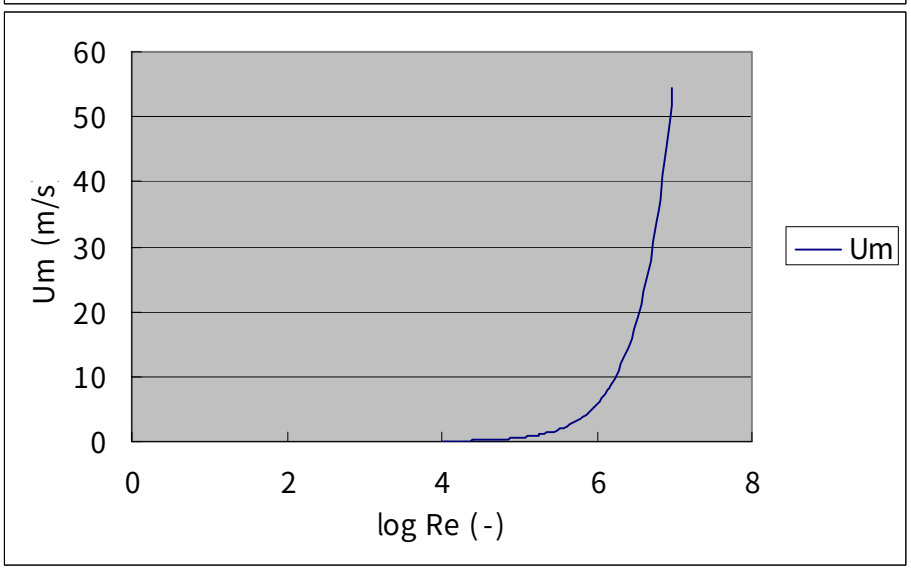

Drag reduction by slip

$(R = 10cm;\ \nu = 1.14\times10^{-6}\ m^2/s;$
$l_x = 100\mu m;\ l_z = 0)$

(1) Drag reduction at high Reynolds number due to slip on the pipe wall was obtained.

(2) Drag reduction is calculated, if the Reynolds number and the slip on the wall are given.

(3) According to the numerical results, a big drag reduction is induced at high Reynolds number.

(4) If the ratio of the slip to the diameter of the pipe is held constant, the bigger drag reduction is obtained at the higher Reynolds number.

3. Exp. Ver. Of Friction Reduction

Artificially made **Superhydrophobic Surface**

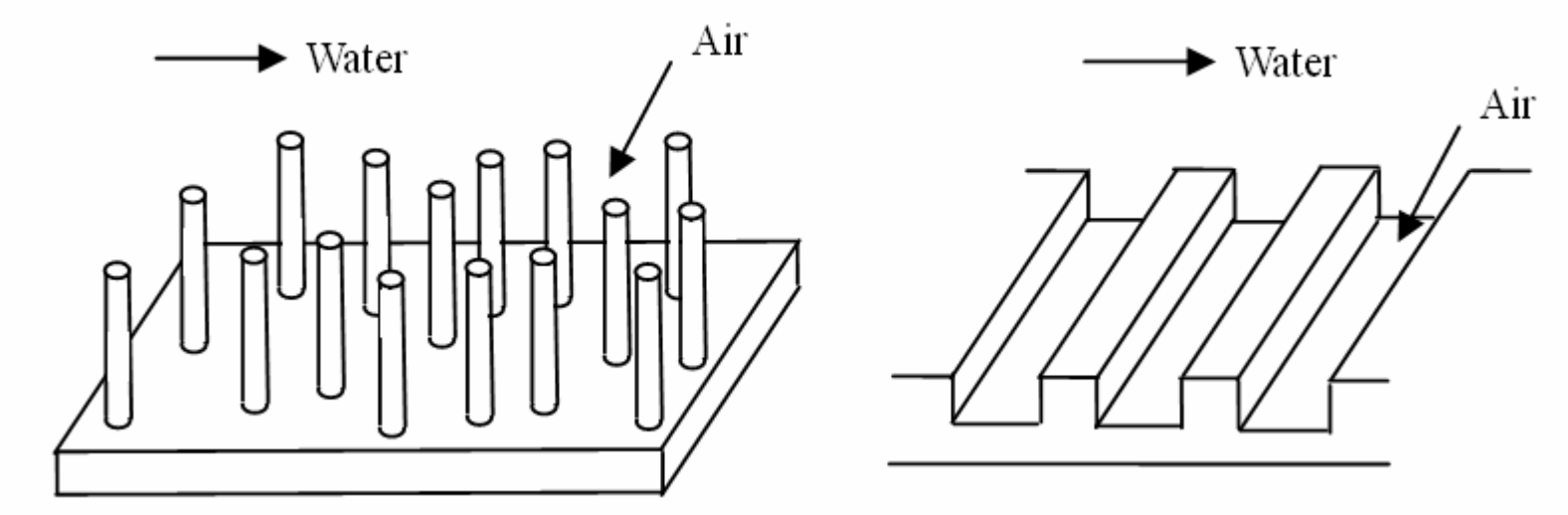

Pillar or post

Ridge or ditch

The logitudinal dirction of the ridges could be in streamwise direction.

Definition of slip length

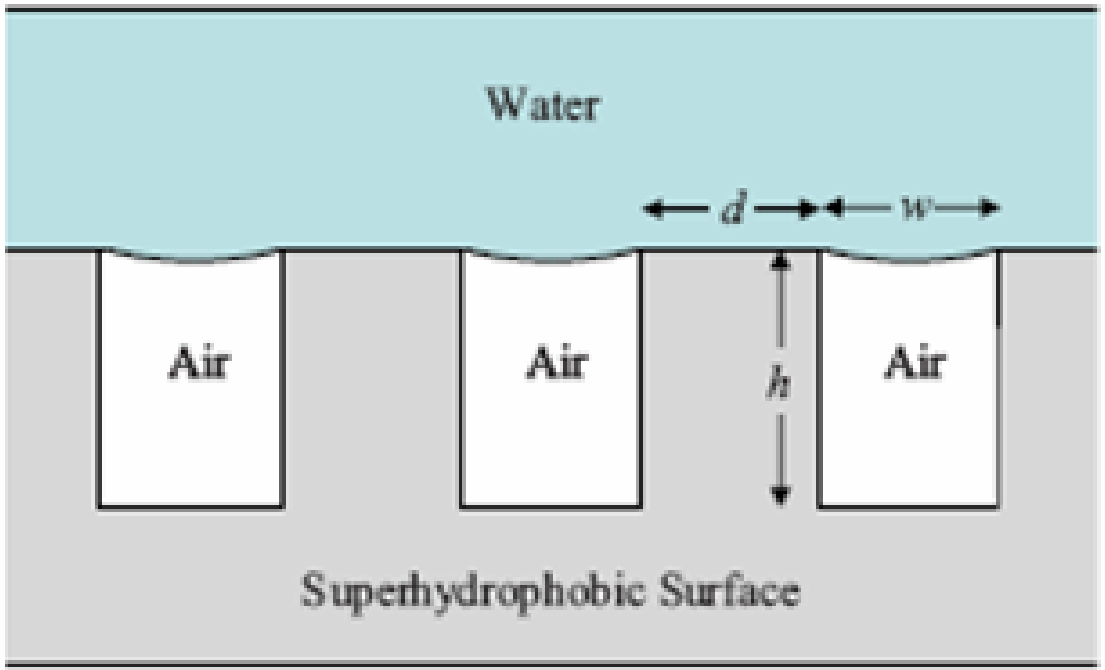

Relationship on the interface of water-air layer

$$u_0 = b \left. \frac{du}{dy} \right|_{y=0}$$

b : slip length

3.1. Experimental results by Lee et al. of POSTECH [2]

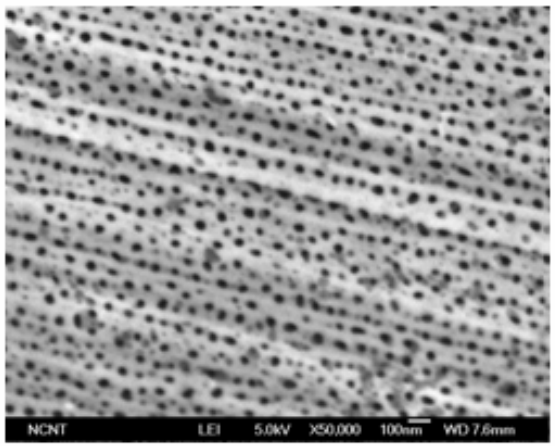

Specimen 1
(nanofiber diameter: 20-30nm)

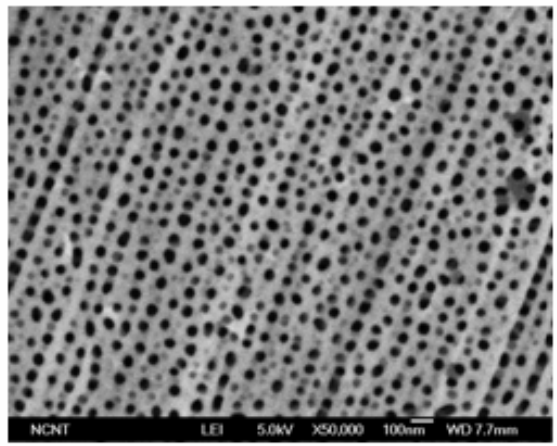

Specimen 2
(nanofiber diameter: 50-60nm)

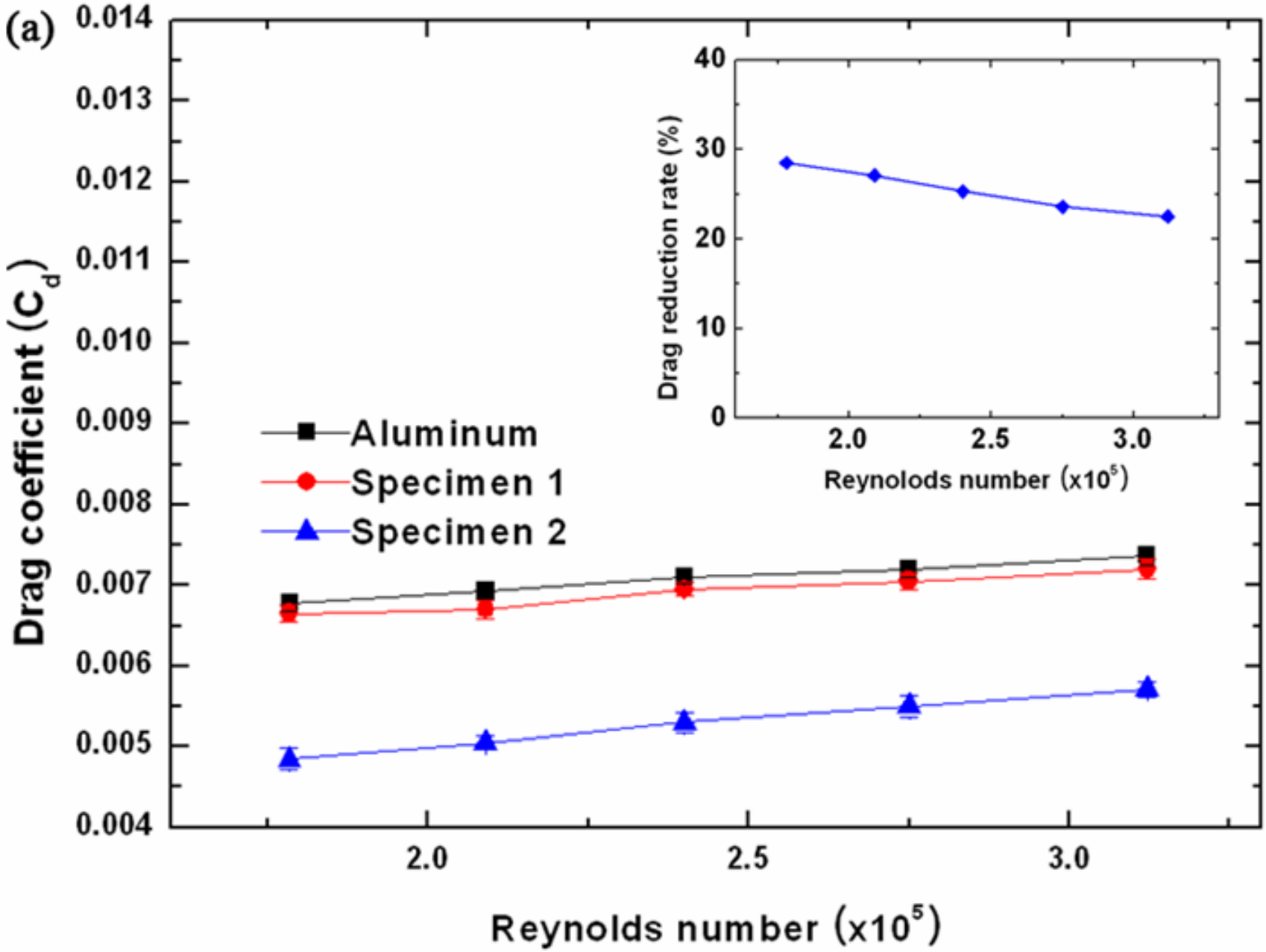
(a)
Drag coefficient (C_d)
0.014
0.013
0.012
0.011
0.010
0.009
0.008
0.007
0.006
0.005
0.004
2.0
2.5
3.0
Reynolds number (x10^5)
Aluminum
Specimen 1
Specimen 2
Drag reduction rate (%)
40
30
20
10
0
2.0
2.5
3.0
Reynolds number (x10^5)

3.2. Experimental results by Daniello et al. of Univ. of Massachusetts [3]

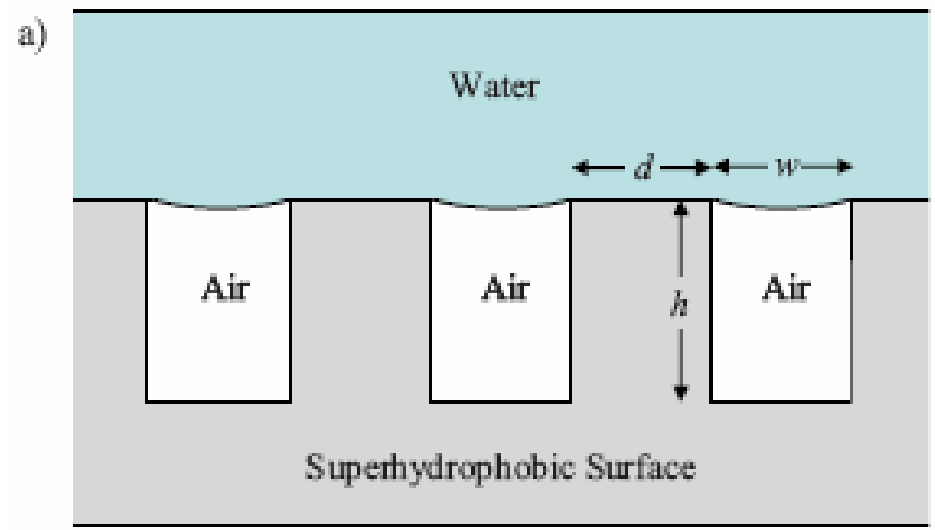

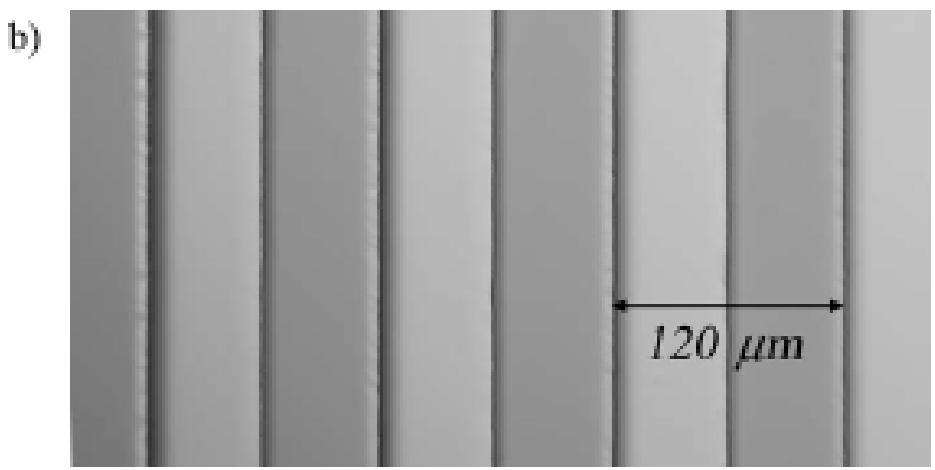

$$d = w = 60 \, or \, 30 \mu m$$

$$h = 25 \mu m$$

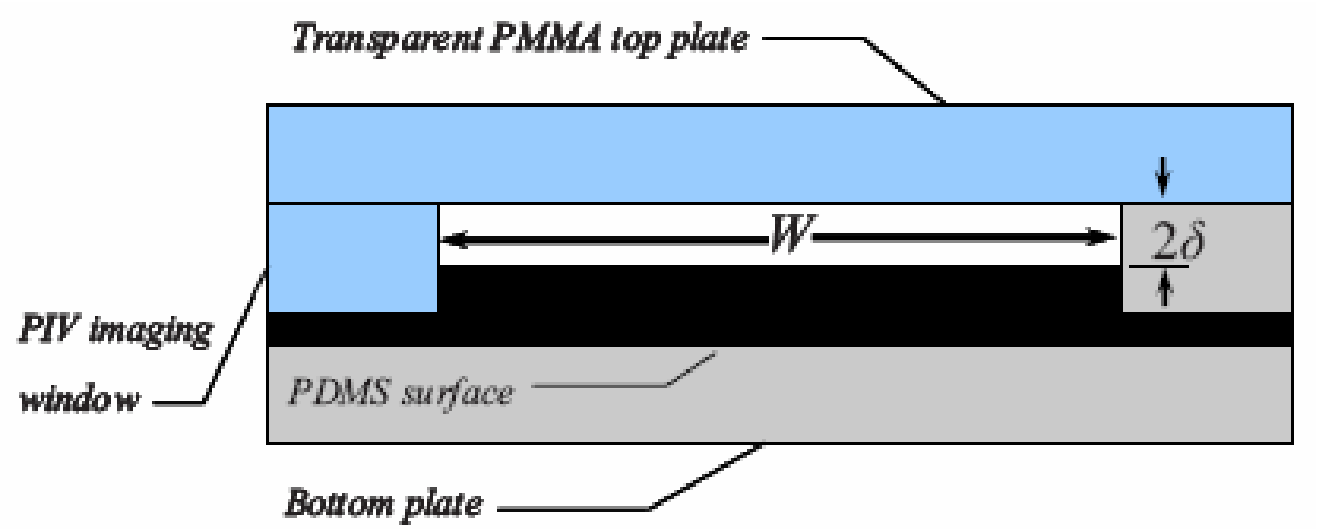

Measurement for velocity distribution

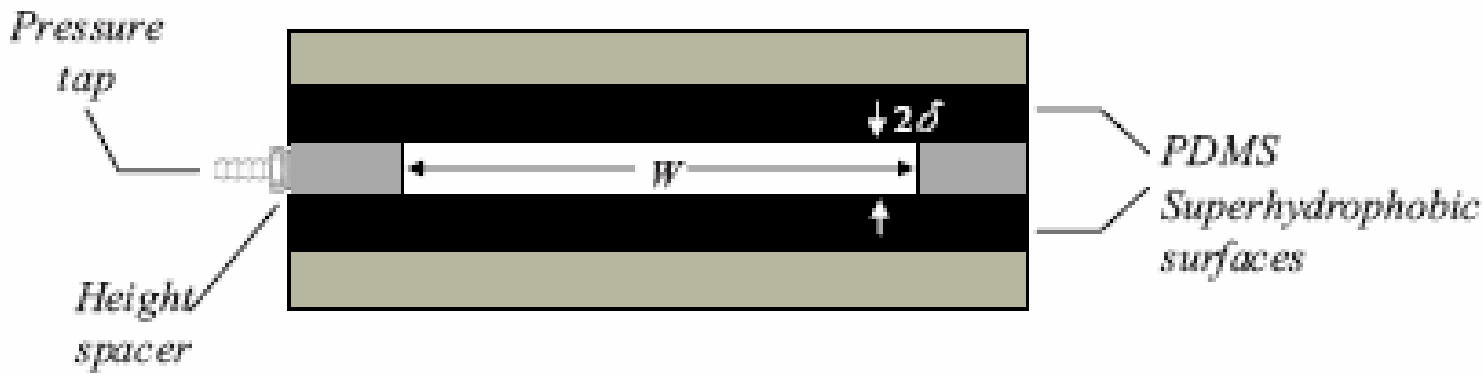

Measurement for pressure drop

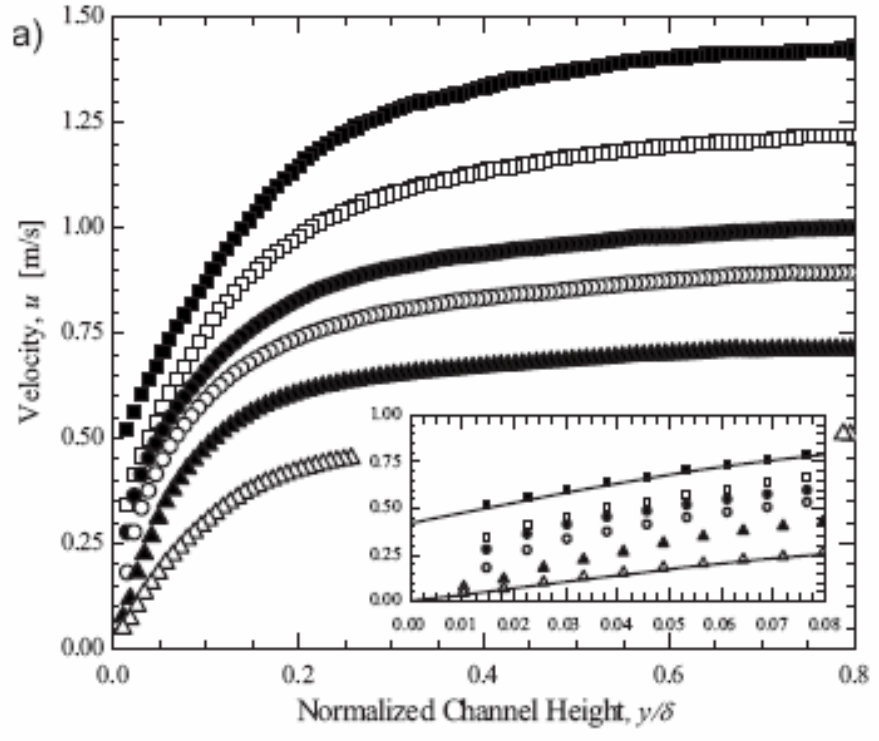

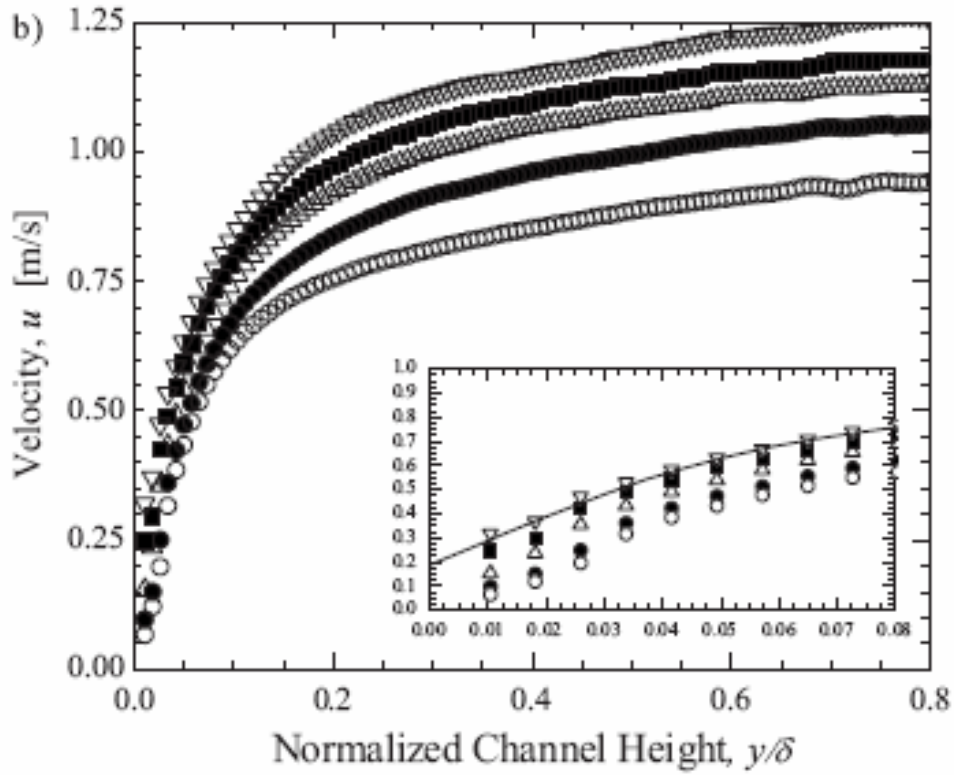

Vel. profile $(d = w = 60\mu m)$

Vel. profile $(d = w = 30\mu m)$

Reynolds number
■ 8200, □ 6960,
● 5150, ○ 4840,
▲ 3900, △ 2700,

Reynolds number
▽ 7930, ■ 7160,
△ 6800, ● 5400,
○ 4970

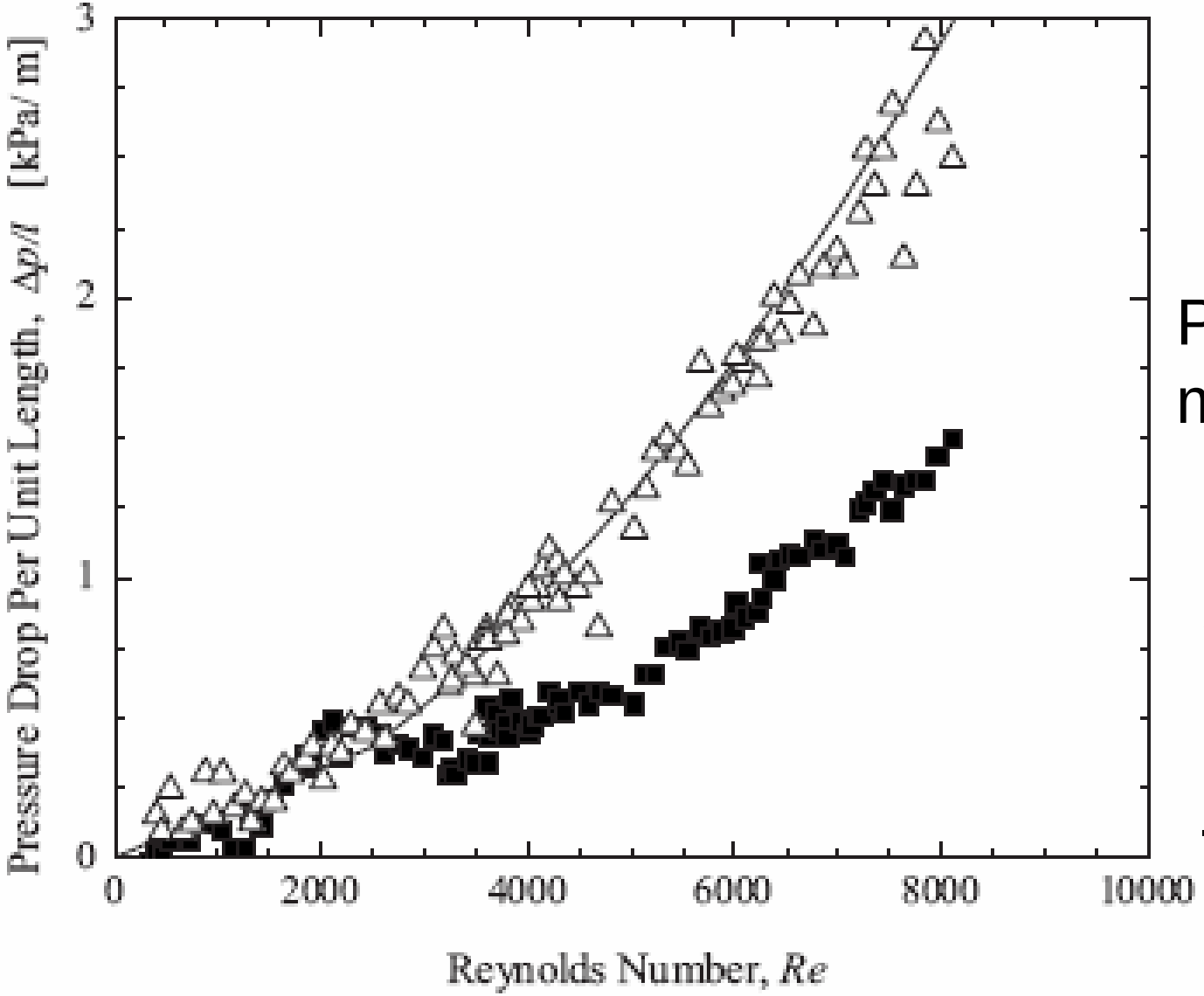

Pressure drop measurements

$(d = w = 60\mu m)$

△: smooth walls

■: two super-hydrophobic surfaces

—: Colebrook line

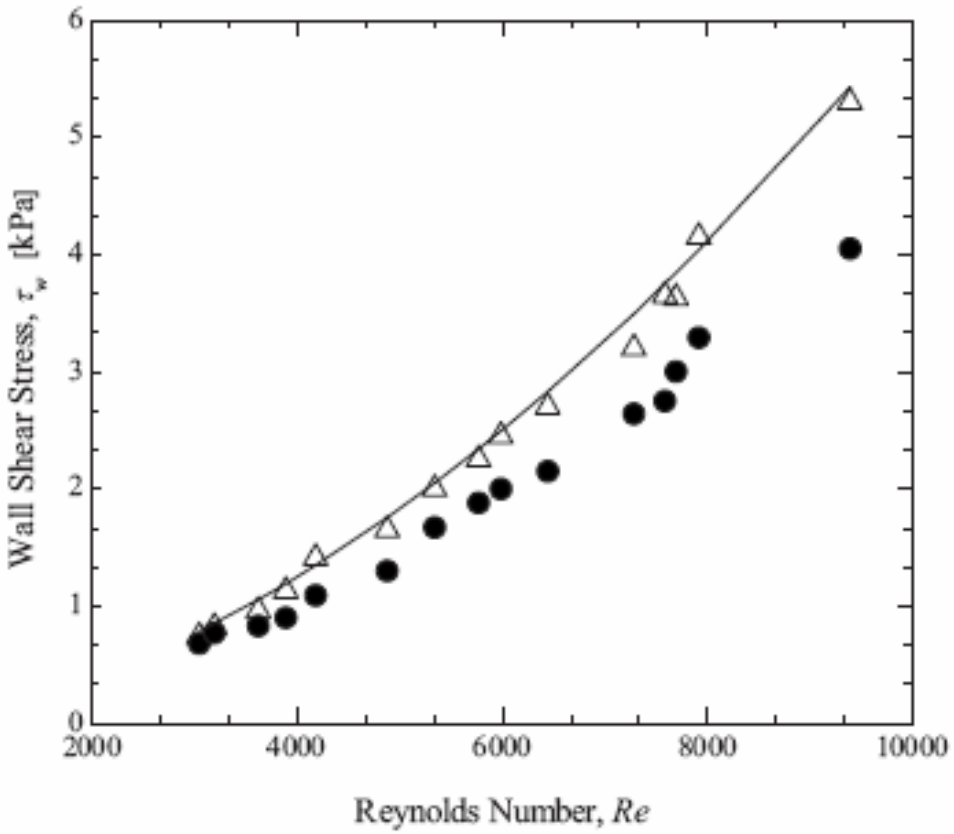

Wall shear stress measured by PIV for a channel of single superhydrophobic surface

$(d = w = 30\mu m)$

△: smooth top wall

●: superhydrophobic bottom surface

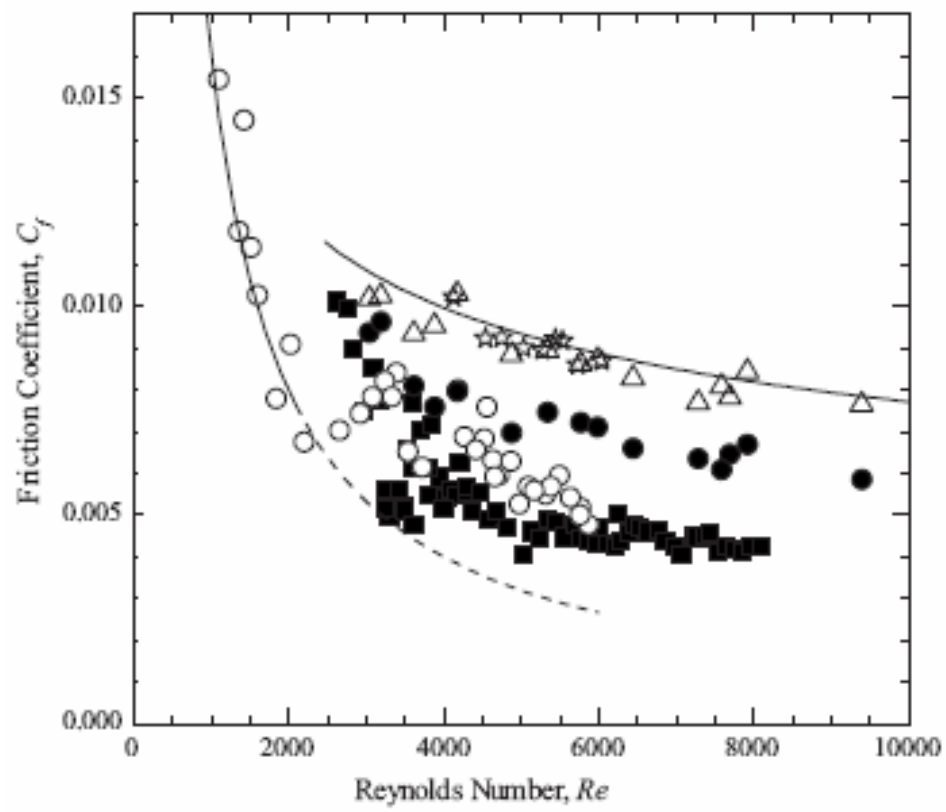

Friction coefficient by PIV and pressure drop.

△: smooth surface

$(d = w = 30\mu m)$

●: superhydrophobic surface

$(d = w = 30\mu m)$

○: superhydrophobic surfaces

$(d = w = 30\mu m)$

■: suphydrophobic surfaces

$(d = w = 60\mu m)$

4. Conclusions

(1) Drag reduction at high Reynolds number due to slip on micro channel wall has been verified experimentally.

(2) A big drag reduction is induced at high Reynolds number.

(3) The bigger drag reduction is obtained at the higher Reynolds number.

(4) Drag reduction is calculated, if the Reynolds number and the slip length on the wall are given.

(5) The estimation of the slip length has not yet been solved fully.

… Conclusions (2)~(3) surprisingly coincides with those obtained by Yoon and Isshiki presented at 2009 SNAK Spring Meeting.

5. Future Directions

(1)Clarification of **mechanism in the vicinity of the body surface**
- theoretical, numerical, experimental
- relation between pillar dimension ~ slip length

(2) Micro pillars or ditches **design technology** (not only for flat plate)

(3) **Durability** of micro pillars and **productionTechnology** in Laboratory level

References

[1] V. Paunov, “Self-Cleaning Surfaces: Virtual Realities,” Nanotechnology lecture,

[2] S. Lee, J. H. Kang, S. J. Lee and W. B. Hwang, “Tens of Centi-Meter Scale Flexible Superhydrophobic Nanofilter Structures Through Curing Process,” Lab on a chip, (2009).

[3] R. J. Daniello, N. E. Waterhouse and J. P. Rothstein, “Drag Reduction in Turbulent Flows over Superhydrophobic Surfaces,” Physics Fluids **21**, 085103 (2009).

[4] K. Fukagata and N. Kasagi, A Theoretical Prediction of Friction Drag Reduction in Turbulent Flow by Superhydrophobic Surfaces, 18, 051703, Physics Fluids, (2006).

[5] B. S. Yoon and H. Isshiki, “Theoretical Prediction of Friction Drag Reduction by Super-Hydrophobicity on Pipe Flow,” SNAK Spring Meeting (2009).